Eur Spine J (2017) 26:2629–2641
DOI 10.1007/s00586-017-5253-x

ORIGINAL ARTICLE

A more realistic disc herniation model incorporating compression, flexion and facet-constrained shear: a mechanical and microstructural analysis. Part II: high rate or 'surprise' loading

Zhi Shan[1] · Kelly R. Wade[2] · Meredith L. Schollum[2] · Peter A. Robertson[3] · Ashvin Thambyah[2] · Neil D. Broom[2]

Received: 18 January 2017 / Accepted: 1 August 2017 / Published online: 8 August 2017

Abstract

Purpose Part I of this study explored mechanisms of disc failure in a complex posture incorporating physiological amounts of flexion and shear at a loading rate considerably lower than likely to occur in a typical in vivo manual handling situation. Given the strain-rate-dependent mechanical properties of the heavily hydrated disc, loading rate will likely influence the mechanisms of disc failure. Part II investigates the mechanisms of failure in healthy discs subjected to surprise-rate compression while held in the same complex posture.

Methods 37 motion segments from 13 healthy mature ovine lumbar spines were compressed in a complex posture intended to simulate the situation arising when bending and twisting while lifting a heavy object at a displacement rate of 400 mm/min. Seven of the 37 samples reached the predetermined displacement prior to a reduction in load and were classified as early stage failures, providing insight to initial areas of disc disruption. Both groups of damaged discs were then analysed microstructurally using light microscopy.

Results The average failure load under high rate complex loading was 6.96 kN (STD 1.48 kN), significantly lower statistically than for low rate complex loading [8.42 kN (STD 1.22 kN)]. Also, unlike simple flexion or low rate complex loading, direct radial ruptures and non-continuous mid-wall tearing in the posterior and posterolateral regions were commonly accompanied by disruption extending to the lateral and anterior disc.

Conclusion This study has again shown that multiple modes of damage are common when compressing a segment in a complex posture, and the load bearing ability, already less than in a neutral or flexed posture, is further compromised with high rate complex loading.

Keywords Ovine lumbar motion segments · Surprise-rate compression · Complex posture · Microstructural analysis · Annular disruption · Mechanism of herniation · Intervertebral disc · Herniation · Radial fissure · Mechanics

Introduction

Part I demonstrated the dramatic effect that a complex posture incorporating physiological amounts of flexion and shear has on both the failure load and failure morphology on a disc subjected to overloading. However, with velocity being the strongest predictor of risk among trunk motion factors in logistic regressions performed on more than 400 repetitive industrial lifting jobs [1], and in vitro tests on ovine motion segments held in a flexed posture demonstrating the critical role of loading rate in the aetiology of herniation [2, 3], it seems pertinent to understand how loading rate might influence the failure of discs held in a complex posture. Part I used a compression rate of 40 mm/min, equating to a test duration of around 5 s, much slower

✉ Meredith L. Schollum
meredith.schollum@auckland.ac.nz

Neil D. Broom
nd.broom@auckland.ac.nz

1 Department of Orthopaedic surgery, Sir Run Run Shaw Hospital, Zhejiang University, Hangzhou, China

2 Tissue Mechanics Laboratory, Department of Chemical and Materials Engineering, University of Auckland, Auckland, New Zealand

3 Department of Orthopaedic Surgery, Auckland Hospital, Auckland, New Zealand

than would be expected in a typical in vivo manual handling situation. Electromyographic studies have shown that between 0.5 and 1 s is required for the muscles of the spinal column to generate a response to a 'surprise' imposition of load [4, 5] and this would equate to an ~tenfold increase in loading rate over that used in Part I.

Although there is evidence for loading rate having an influence on disc failure mode, the controlling mechanisms are less clear. It is well established that heavily hydrated connective tissues such as the intervertebral disc and articular cartilage display strong strain-rate-dependent mechanical properties [6–8] and this derives from their ultra-low permeabilities restricting the ease with which matrix water can be driven out under an under an applied deformation or strain. The more rapidly this is applied, the greater the induced stress for a given strain with the potential for additional mechanisms and degrees of disruption.

The aim of this new study was to use the same complex loading employed in Part I but with a compressive rate an order of magnitude higher, so as to investigate how a more realistic posture and loading rate might influence disc failure.

Methods

Lumbar spines from female sheep, 2–4 years in age and thus with either partially or fully closed growth plates (i.e., mature or nearly so), were collected immediately following killing and stored for up to 6 months at −28 °C. There was no evidence of degeneration in any of the lumbar spines based on a macroscopic inspection of the transected discs. As described in Part I, the ovine lumbar spine is a well-accepted model for biomechanics studies.

As before, these ovine motion segments were subjected to flexion with an offset compression causing translation/shear limited by the facet joints. Our objective was to simulate the situation arising when bending and twisting while lifting a heavy object, and thus involving elements of flexion, lateral bending, axial rotation, anterior–posterior shear and lateral shear. Thus, discs were subjected to an offset compression whilst rotated to drive the disc to its limits of motion, constrained (or governed) by the facet joints and then compress it to failure in this posture (Fig. 1).

Each potted motion segment was positioned in the rig with its long axis tilted laterally 20° to the machine compression axis (see Fig. 1c, d) as a means of applying a component of lateral shear to the motion segment when compressed. The segment was then rotated 5° anti-clockwise as viewed from above (see Fig. 1e, f) about its long axis. Finally, 7° of flexion, approximately the limit of physiologic flexion for ovine discs [9], was applied in the plane corresponding to the original sagittal plane of the motion segment before it was rotated (see Fig. 1a, b). The flexion in this plane, being offset to the disc's sagittal plane, had the effect of adding a small component of lateral bend.

By retaining the facet joints, we intended to ensure that the disc was constrained to an approximation of physiologic loading as in previous investigations [3, 10]. The result was a complex posture consisting of elements of flexion, and translation involving anterior–posterior shear and lateral shear which, therefore, would also include a small amount of lateral bending and axial rotation. Shear and bending measurements were obtained using two video cameras appropriately positioned with respect to the primary axes of rotation—see the overlaid initial and post-test images in Fig. 1a, c. Similar to the low rate study in Part I, average induced shear was 4.1 ± 0.7 mm to the right hand side, 2.2 ± 0.6 mm anteriorly, and with the opened left facet unable to provide sufficient constraint, a net lateral bend to the left of 1.3° ± 0.2°.

The compression rate was increased to 400 mm/min (referred to as 'high rate') ensuring a crosshead displacement of around 3 mm within 0.5 s to produce motion segment failure at a "surprise" rate of loading [3].Samples were compressed using an Instron materials testing machine under load control and test termination criteria were adopted from previous studies [3, 10] set at either 15% load drop or a driven displacement of 3 mm, whichever came first. As before, these criteria were selected based on preliminary trials and were intended to accommodate both the accuracy of the control system of the Instron and the natural variation in the samples and the combination of these factors produced a range of levels of damage, also consistent with previous investigations [3, 10].

For this high rate study, 37 motion segments from 13 spines were tested. Based on examination of the load–displacement curves, 7 tests were terminated prior to any drop in load (early stage) thus providing a useful insight to the initial stages of disc disruption. Generalised load–displacement plots were of the same type as those published in flexion overload studies [3, 10]. Following testing, each motion segment was trimmed to isolate the disc and its adjacent endplates, fixed for 7 days in 10% formalin and decalcified for 21 days in 10% formic acid as in previous studies [3, 10]. Each sample was then bisected sagittally and cryosectioned to obtain 30 μm thick sections along one of the two planes (Fig. 1g, h; Table 1) namely (1) the '45° sagittal plane' (22 samples) which minimised trimming losses of the central posterior and lateral annulus, as well as encompassing the anterior annulus, and (2) the 'sagittal plane' (15 samples), a commonly used plane that allowed

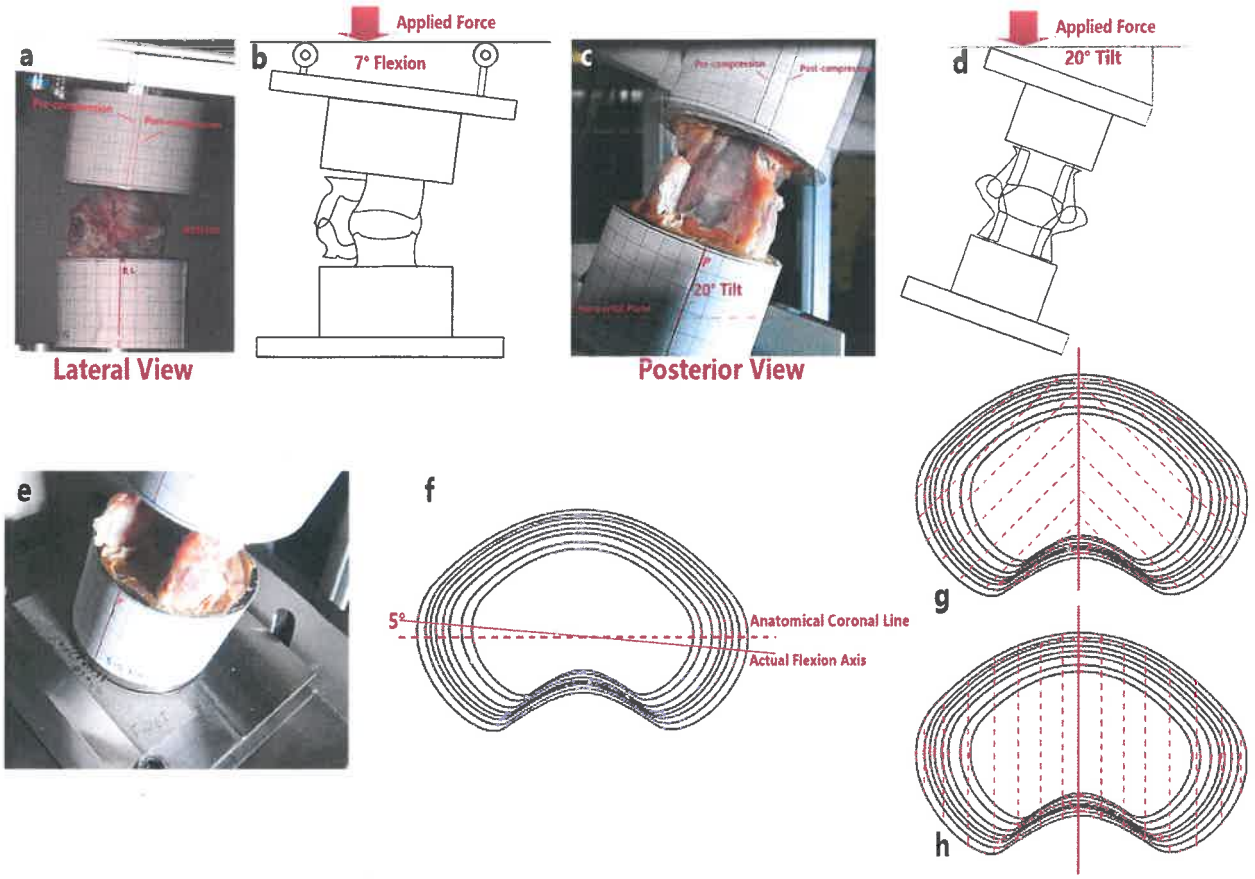

Fig. 1 The complex posture incorporated 7° of forward flexion (**a**, **b**), a 20° right lateral tilt (**c**, **d**), and a 5° anticlockwise rotation of the motion segment in the rig (**e**, **f**). Note the offset flexion axis adds an element of right lateral bend. When compressed the translation/shear is governed by the facet joints. (**a**, **c**) Overlaid images of pre- and post-compression of the same segment from lateral and posterior views, respectively. **g**, **h** Indicate the two section planes employed: 45° sagittal and sagittal

direct comparison with earlier studies [9, 12]. Slices were microscopically analysed in their fully hydrated state using DIC (Differential Interference Contrast) optical microscopy. With a 0.7 mm interval, between 12 and 18 sections were examined per half disc block.

As described in Part I, failure modes were recorded according to type, (listed and illustrated schematically in Fig. 2).

All data obtained were compared with the 'low rate' complex loading study (Part I), and with previous studies using simple flexion at the same 'low' and 'high' rates [3, 10]. The severity of annular damage between the left and right halves of each disc in this study was assessed and assigned a damage score. Noting that all structural observations were obtained from sections cut either sagittally or at 45°, any comparison of damage scores between left and right was always made on the same disc to eliminate this section plane effect. Damage scores were first averaged for three slices per disc half, then the 37 scores for each side were statistically analysed using the paired t test.

Independent t test or Analysis of Variance was used to compare mean data among groups, with differences between groups analysed using the Least Significant Difference post hoc analysis. Statistical analyses were performed using SPSS 21.0 (IBM Corp., Armonk, NY, USA). $P < 0.05$ was considered significant.

Results

Mechanical observations

The bony structures of the facet joints of all 37 segments survived the test intact, indicating that the complex loading that was applied at the high rate did not exceed their physiologic limit. It should also be noted that previous investigations indicate that 7° of flexion on its own is well below that required to damage the disc [3, 10].

Table 2 lists the failure loads for samples subjected to the complex loading together with previously obtained failure

Table 1 Details of damage after 400 mm/min compression loading in a complex posture; samples 1–7: tests stopped at an early stage of failure. Samples 8–37: tests with gross failure as indicated by a drop in applied load

	Sample	Section plane	Damage modes presented				Location of annular damage	Illustrated in figure
			V	M_d	M_{nc}	ET		
1	CL400 2 L1-2	Sag		•	•		Post + PLat + Ant	
2	CL400 2 L5-6	Sag		•	•		Post + PLat + Ant	
3	CL400 3 L1-2	Sag			•		Post	
4	CL400 3 L3-4	Sag	•				Post + PLat	Figure 5d
5	CL400 4 L1-2	Sag		•	•		Post + PLat	
6	CL400 4 L3-4	Sag		•	•		Post + PLat + Ant	
7	CL400 8 L5-6	45Sag	•	•	•	•	Post + PLat + Lat + Ant	
8	CL400 1 L3-4	Sag		•	•	•	Post + PLat + Ant	Figure 7
9	CL400 1 L5-6	Sag		•	•		Post + PLat + Ant	
10	CL400 2 L3-4	Sag		•	•		Post + PLat + Ant	
11	CL400 3 L5-6	Sag	•	•	•		Post + Plat	
12	CL400 4 L5-6	Sag		•	•		Post + PLat + Lat + Ant	
13	CL400 6 L1-2	45Sag	•	•	•		Post + PLat + Lat	
14	CL400 6 L3-4	45Sag	•	•	•	•	Post + PLat + Lat + Ant	
15	CL400 6 L5-6	45Sag		•	•		Post + PLat + Lat + Ant	
16	CL400 7 L1-2	45Sag		•	•	•	Post + PLat + Lat + Ant	
17	CL400 7 L3-4	45Sag		•	•	•	Post + PLat + Lat + Ant	
18	CL400 7 L5-6	45Sag		•	•	•	Post + PLat + Lat + Ant	
19	CL400 8 L1-2	45Sag	•		•		Post	
20	CL400 9 L1-2	45Sag	•	•	•		Post + PLat + Lat	
21	CL400 9 L3-4	45Sag	•	•	•		Post + PLat + Ant	
22	CL400 9 L5-6	45Sag	•	•	•	•	Post + PLat + Lat + Ant	
23	CL400 10 L1-2	45Sag		•	•		Post + PLat + Lat + Ant	Figure 3
24	CL400 10 L3-4	45Sag		•	•	•	Post + PLat + Lat + Ant	Figure 4
25	CL400 10 L5-6	45Sag	•	•	•		Post + PLat + Lat + Ant	
26	CL400 11 L1-2	45Sag	•	•	•		Post + Plat	Figure 5a–c
27	CL400 11 L3-4	45Sag	•	•	•	•	Post + PLat + Lat + Ant	
28	CL400 11 L5-6	45Sag	•	•	•		Post + PLat + Lat	
29	CL400 12 L1-2	Sag		•	•		Post + PLat + Ant	Figure 5
30	CL400 12 L3-4	Sag	•	•	•		Post + PLat + Ant	
31	CL400 12 L5-6	Sag		•	•		Post + PLat + Ant	
32	CL400 13 L1-2	Sag	•	•	•		Post + PLat + Ant	
33	CL400 13 L3-4	45Sag		•	•		Post + PLat + Lat + Ant	
34	CL400 13 L5-6	45Sag	•	•	•		Post + PLat + Lat + Ant	
35	CL400 14 L1-2	45Sag		•	•	•	Post + PLat + Lat + Ant	
36	CL400 14 L3-4	45Sag	•	•	•	•	Post + PLat + Lat + Ant	
37	CL400 14 L5-6	45Sag	•	•	•		Post + PLat + Ant	

V vertebral fracture, M_d direct mid-span tear, including the outer wall, M_{nc} non-continuous mid-span tear, *ET* annulus–endplate tear, *Post* posterior, *Plat* posterolateral, *Lat* lateral, *Ant* anterior

load data for similar motion segments overloaded in either 'low rate' complex loading (see Part I) or in simple flexion at both 'high rate' and 'low rate' [3, 10]. The average peak failure load under 'high rate' complex loading [6.96 kN (STD 1.48 kN)] was significantly lower than 'low rate' complex loading [8.42 kN (STD 1.22 kN)] and simple flexion at either the 'low' or 'high' rate [9.69 kN (STD 2.56 kN) and 9.58 kN (STD 1.96 kN), respectively]. The peak failure load was, on average, higher in the more caudal segments, this difference being significant between L1-2 and L5-6.

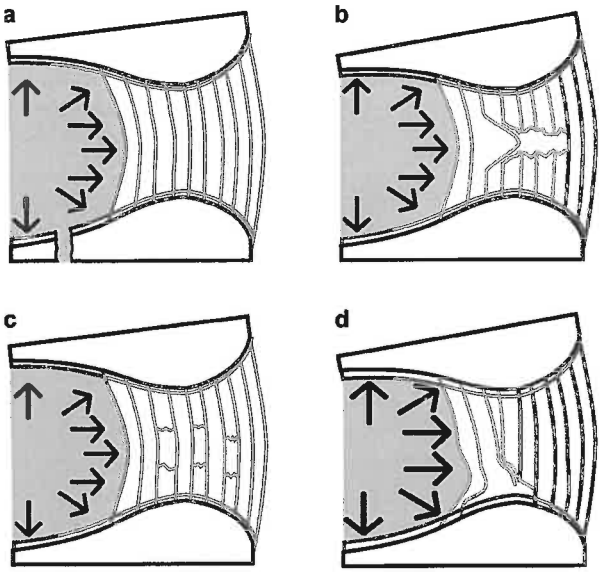

Fig. 2 Motion segments contained one or more of these four types of damage: **a** endplate fracture (*V*) in which the osseous endplate itself was broken and the resulting defect penetrates the vertebral body, **b** mid-span direct tearing (M_d) in which the annular wall suffered rupture spanning several adjacent lamellae, **c** mid-span non-continuous tearing (M_{nc}) in which several alternate lamellae ruptured, and **d** annulus–endplate tears (ET) which involved damage to the annulus–endplate junction

Microstructural analysis of damage

Damage types for all 37 tested motion segments are summarised in Table 1.

General patterns of disruption for tests terminated after peak load

All 30 segments (100%) contained mid-span non-continuous annular tears. Direct radial rupture within the mid-span annulus was present in 29 samples (96.7%). Vertebral endplate fracture occurred in 16 segments (53.3%). Both direct radial tears in the mid-span annulus and vertebral endplate fractures occurred in 15 segments. Disc–endplate junction tears were present in 10 segments (30%). Posterior annular failure involving either M_{nc} or M_d modes, or both, was present in 30 segments (100%), whereas anterior annular failure occurred in 24 segments (80%), again involving both M_{nc} and M_d modes. Annular tearing on the left side of the disc, both anteriorly and posteriorly, was more severe than on the right side (Table 3).

Image sets illustrating damage types

Note, the specific sample for each figure is detailed in Table 1.

Figure 2 shows a series of images from a segment suffering both direct radial and non-continuous tearing. The most central posterior region (Fig. 3a) has the beginnings of a radial tear (hollow arrow) together with non-continuous tearing as evidenced by the alternating intact and ruptured lamellae (solid arrows). In moving slightly laterally to the section in Fig. 3b, the direct radial rupture is now more advanced and this in combination with more non-continuous tearing has increased the disorder of the annular lamellae with inner ruptured elements being swept into the primary breach. Advancing further laterally in Fig. 3c the damage is much less severe, consisting of a series of relatively minor inter-lamellar delaminations having only limited radial connectivity with each other. A significant level of distortion persists in the otherwise largely intact lamellae which appears to be generated by the intrusion of nucleus (see arrow).

Figure 4 illustrates a disc with a direct radial rupture in the mid-span annulus. The central slice in Fig. 4a shows a large pocket in the peripheral annulus that has been filled by displaced nucleus material. Moving more laterally to Fig. 4b, the disc wall is completely ruptured, thus facilitating this nuclear displacement. Advancing laterally still further to Fig. 4c, more nucleus material can be seen retained within the annulus but with some lamellae either side of the displaced nuclear mass still unruptured. This suggests that the nucleus material has both extruded directly through the radial rupture shown in Fig. 4b and also tracked some distance circumferentially between lamellae. Note also the inwards collapse of the medial lamellae in all three images, indicative of a loss of nuclear pressure following the extrusion.

Figure 5a–c illustrates failure involving a combination of direct radial rupture, non-continuous tearing, and endplate fracture. Progressive sectioning showed that the fracture in the superior endplate extended from the posterior right through to the anterolateral aspect (see approximate fracture path marked with an irregular line on schematic inserts). A near complete direct rupture of the posterior annulus is shown in Fig. 5a. More posterolaterally, non-continuous annular damage is indicated by the rupture of alternate lamellae (Fig. 5b). Still more laterally (Fig. 5c) there is only minor delamination of lamellae. Also, nuclear material can be seen extruded through the fracture site visible in Fig. 5b, c (see circled sites). Figure 5d, is from another disc, offering a view of a fracture through the endplate only.

Figure 6 shows one of the 24 segments with radial ruptures extending across multiple lamellae in both the anterior and posterior annulus. The most medial section (see Fig. 6a) showed no indication that nuclear material had been extruded from the posterior and anterior regions, but progressing laterally

Table 2 Comparison of motion segment failure by compression with: a complex posture at high rate (CL400), a complex posture at low rate (CL40)—ref Part I, previously published flexed posture at high rate (F400), and previously published flexed posture at low rate (F40)

	CL400	CL40[a]	F400[b]	F40[c]
Posture	7° flexion, 20° offset compression, 5° axis rotation	7° flexion, 20° offset compression, 5° axis rotation	10° flexion, vertical compression	10° flexion, vertical compression
Loading rate (mm/min)	400	40	400	40
Segments tested (including early stage termination)	30 (37)	21 (30)	16 (24)	19 (24)
Load at failure (kN)	6.96 (STD 1.48) (3.58–9.82)	8.42 (STD 1.22) (5.93–10.92)	9.58 (STD 1.96) (5.92–12.91)	9.69 (STD 2.56) (6.10–15.00)
Prevalence of damage types[d]				
Vertebral fracture	16 (53.3%)	7 (33.3%)	4 (25.0%)	9 (47.4%)
Non-continuous tearing	30 (100%)	21 (100%)	1 (6.3%)	1 (5.26%)
Direct radial tearing	29 (96.7%)	8 (38.1%)	4 (25.0%)	6 (31.6%)
Disc–endplate tearing	10 (33.3%)	9 (42.9%)	9 (56.3%)	3 (15.8%)
Anterior annular tearing	24 (80%)	2 (6.7%)	1 (6.3%)	0 (0%)

Quantitative data are expressed as mean ± standard deviation

[a] Refer Part I. A more realistic disc herniation model incorporating compression, flexion and facet-constrained shear: a mechanical and microstructural analysis. Part I: low rate loading

[b] Data from 'How Healthy Discs Herniate' [10]. Refer to Table 2, 'Neutral + high rate'

[c] Data from 'How Healthy Discs Herniate' [10]. Refer to Table 2, 'Flexed + high rate', endplate failure and disc herniation combined, with five early stage tests (detailed in Table 3) excluded; S1 L1-2, S3 L1-2, S3 L5-6, S8 L3-4, S8 L5-6

[d] Only those tests terminated after peak load were counted

Table 3 Comparison of severity of annulus and endplate damage between left and right side of disc

	Left side	Right side	*P* value
Anterior annulus	1.784 (STD 1.057)	1.279 (STD 0.898)	0.001
Posterior annulus	1.910 (STD 1.011)	1.360 (STD 1.109)	0.004
Disc–endplate tearing	0.460 (STD 0.695)	0.441 (STD 0.681)	0.876
Vertebral fracture	0.216 (STD 0.534)	0.189 (STD 0.397)	0.786
Scores for each type of annular damage	0: No such type of damage presented.		
	1: Single mid-span lamella delamination or circumferential tearing (M_{nc}) (e.g. Fig. 5c)		
	2: Multiple mid-span lamellae delamination or circumferential tearing (M_{nc}) (e.g. Fig. 3a)		
	3: Direct mid-span radial rupture (M_d) across multiple lamellae (e.g. Fig. 4b)		
	4: Direct mid-span radial rupture (M_d) across entire annulus (e.g. Fig. 7b)		
Score for Disc–Endplate tearing	0: No such type of damage presented		
	1: Nucleus–endplate tearing OR annulus–endplate tearing		
	2: Nucleus–endplate tearing AND annulus–endplate tearing		
Scores for each type of endplate damage	0: No such type of damage presented		
	1: Fracture contained within endplate (e.g. Fig. 5d)		
	2: Fracture of endplate and vertebrae (e.g. Fig. 5a–c)		

Quantitative data are expressed as mean ± standard deviation

there is clear evidence of such extrusion especially through the anterolateral annular rupture (see Fig. 6b, c).

Figure 7 illustrates damage involving annulus–endplate tearing (observed in 11 segments). The most medial image (Fig. 7a) shows the tear extending from the nucleus region (small arrow) to at least the mid-annulus (hollow arrow). Moving progressively laterally, we can see that this endplate tear reverts to a more direct mid-span annular rupture (Fig. 7b). Image Fig. 7c indicates that advancing even more laterally the endplate tear is less extensive with both direct mid-span rupture and circumferential delamination dominating the damage modes. This image also shows a mass of completely detached nuclear material that has been extruded through

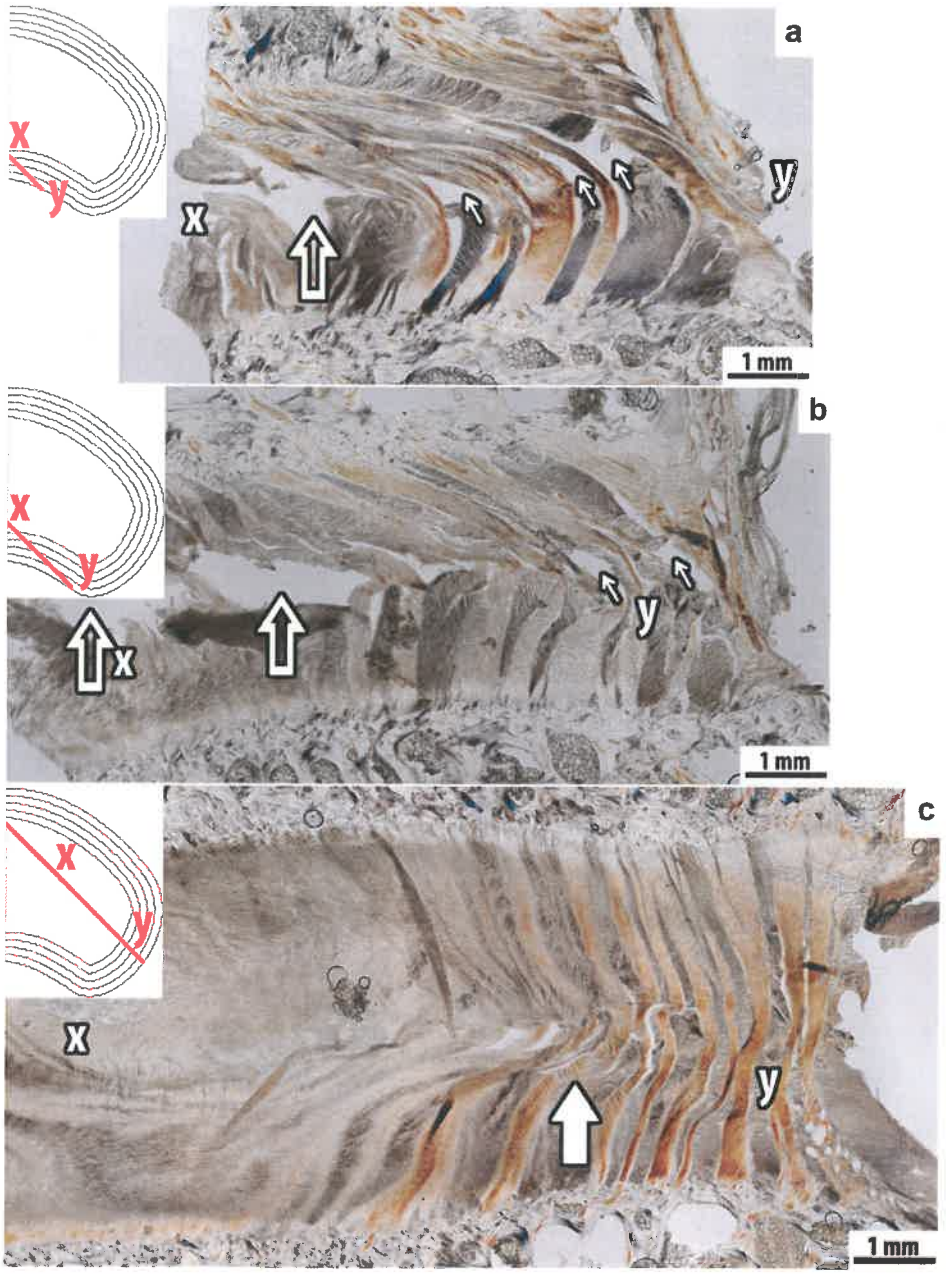

Fig. 3 A disc with circumferential tearing (*solid arrows*) and direct tearing (*hollow arrows*). **a** Predominantly tearing of alternate lamellae in the posterior central region. **b** The radial tear connects to the inner annulus in a further lateral section. **c** Damage persists further laterally as delamination and distortion (see *arrow head*). Note that the *x* and *y* in image indicate the orientation of cutting plane

the posterolateral rupture but contained within the posterior ligament (solid arrow).

Discussion

This study has shown that not only are multiple modes of damage common when compressing a segment in a complex posture but also that the disc–endplate system is particularly vulnerable to damage when rapidly loaded in a complex posture. The load at failure was significantly lowered, and unlike simple flexion or low speed complex posture loading, direct radial ruptures and circumferential failure (evidence from non-continuous tearing) in the posterior and posterolateral regions were commonly accompanied by disruption extending to the lateral and anterior disc wall. Anterior concentric tears have been reported in 75% of human L4-5 discs [11], as well as

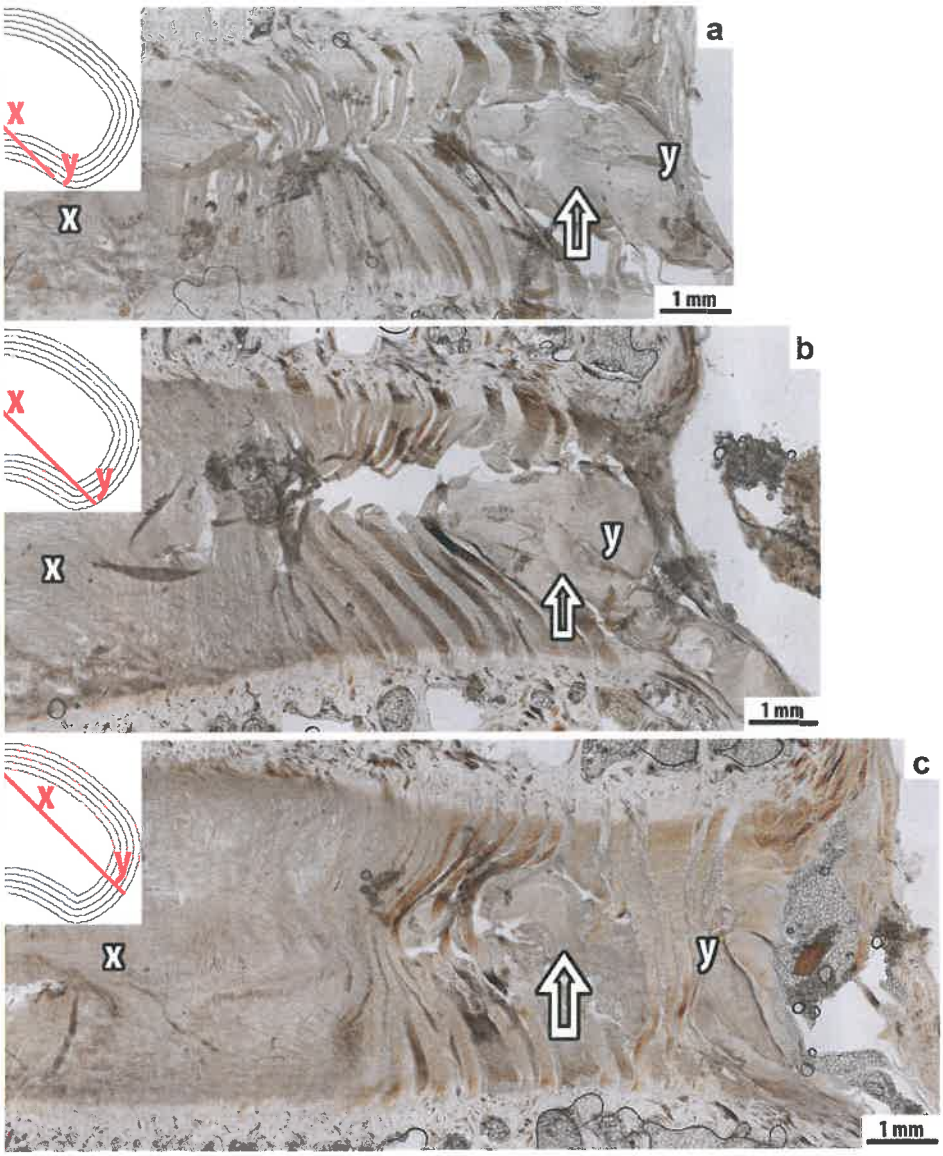

Fig. 4 A disc that experienced mid-span annular direct tearing. **a** The central posterior region of the disc, a pocket of nuclear material can be found within the peripheral annulus (*hollow arrow*). **b** A path of protrusion through the inner annulus in the posterolateral annulus. **c** The pocket of nucleus material extends circumferentially to the lateral region of the disc

anterior radiating tears in 47% of 10–30-year olds and in more than 75% of 51–80-year olds. This suggests that the complex posture and high rate loading employed in the present study and resulting in disruption of the anterior annulus may well have clinical relevance.

Researchers have determined that the damage caused by flexion usually occurs in the posterior and posterolateral regions of the disc (~4–8 o'clock region shaded in Fig. 8a). But, as noted in Part I, it has been shown very recently that in the flexed posture nucleus material commonly migrates into the lateral annulus before tracking circumferentially within the annulus [12]. This is likely due to the anterior shear generated with the flexed posture causing one set of the oblique–counter oblique fibres to be more engaged in load bearing than the other, thus increasing the probability of overload failure of the lateral region. The location of this lateral damage highlights how vulnerable the disc is to loading scenarios that engage to a greater degree one set of oblique–counter oblique lamellae.

In the current study, we have lateral and anterior movement of the superior vertebrae (Fig. 8c), resulting in a shear direction approximately 30° from the coronal plane

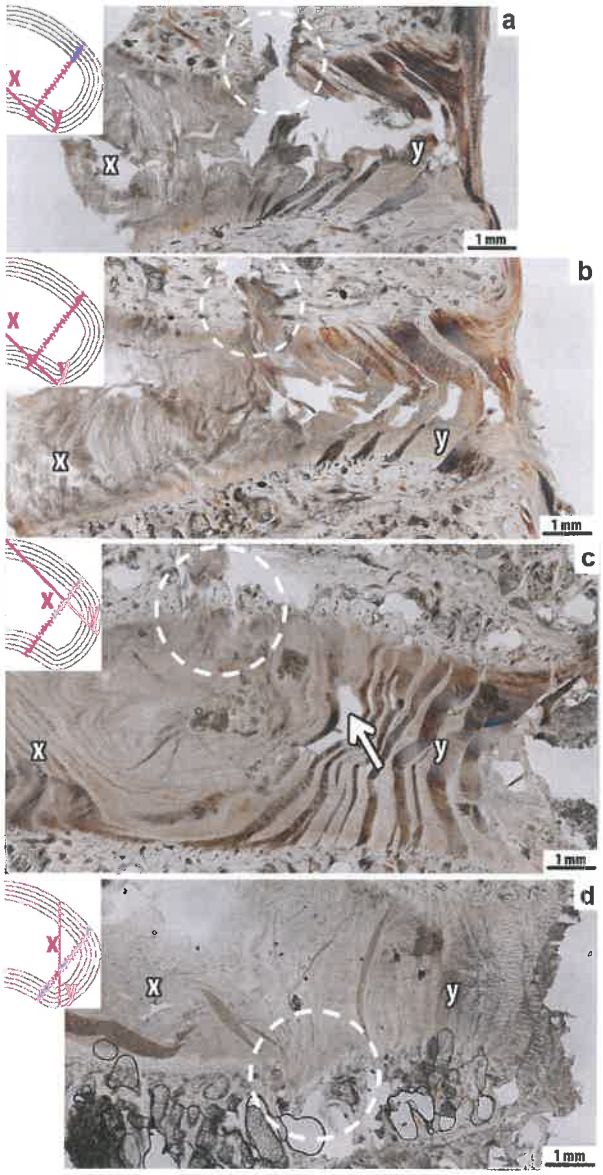

Fig. 5 **a–c** A disc with both vertebral and annular failure. The posterior wall has a direct tear in addition to superior vertebral fracture (**a**). Moving laterally, the annular tear presents as a circumferential tear then delamination, and the fracture continues (**b, c**). A slice taken from a different segment (**d**) contains a shallow fracture, through the endplate only

(Fig. 8a). The preferential loading of one counter-oblique fibre set occurs in the annular regions perpendicular to the shear direction, illustrated schematically in Fig. 8a (dotted regions ~4–5 o'clock on right and ~10–11 o'clock on left of the figure). The span of affected annular wall on the left is approximately double the length of that on the right side, and rather than overlapping with the region of damage induced by flexion, it could potentially connect with it, creating a more extended region of structural weakening on left side of the disc. In fracture mechanics terms, for a given level of applied loading, a larger-sized region of localised structural weakening will render the component more vulnerable to potential failure than a smaller one. This principle might well account for the more severe annular damage reported in the LH (left hand) annulus compared to the RH (right hand)(detailed in Table 3). With the same complex posture at the 'low' rate of compression, anterior annular damage was rare and non-continuous tearing was more common or even exclusively on the RHS in 10/30 of the discs (see Part I). This was attributed to more stress on the loaded set of lamellae on this side due to the left lateral bend in conjunction with the right lateral shear. The contrary damage at the high loading rate, as well as frequent damage in the anterior wall is clear evidence that loading rate does influence the mechanics of failure. We suggest that with less time for fluid pressure equalisation at the 'high' rate, the extra length of wall parallel to the shear direction on the LHS is critical.

Previous research [13] demonstrated that bending in an axial plane 30° to the sagittal plane directed the movement of the nucleus toward the other side of the disc. In the current study, the motion segments were also bent asymmetrically (5° offset towards right, Fig. 1), and the annular damage on the left side was more severe. Perhaps the lack of time for fluid pressure to more evenly dissipate results in the asymmetric movement of nucleus becoming a factor at high rates of loading.

An increased frequency of endplate fracture was observed in the present study compared to that found with either low rate complex loading or simple flexion (Table 2). In the present study, nearly half of the samples presenting with annular wall damage ultimately failed by vertebral endplate fracture. It is unlikely that vertebral endplate fracture occurred first, with almost all of the segments with endplate fracture showing annular tears, but not vice versa. We intuit that the influence of the high rate is dominant here. With less time for the structural elements in the hydrated disc to re-adjust viscoelastically to the internal force trajectories generated by the applied compression in the complex posture, higher internal stresses will be developed (both hydrostatic in the nucleus and tensile in the annulus) putting additional elements at risk, including the rigid endplate tissue.

Like Berger-Roscher [14], we have described complex postures increasing the risk of failure, though their more severe posture, and a loading protocol of 1000 cycles at 2 Hz led to more endplate junction failures (76%) and no herniations. In our high rate acute overload model, the complex posture appears to compromise the disc wall, generating fewer endplate junction failures than reported for high loading rate and 10° flexion [3] (see Table 2; 33.3 versus 56.3% incidence). If we consider the annular–

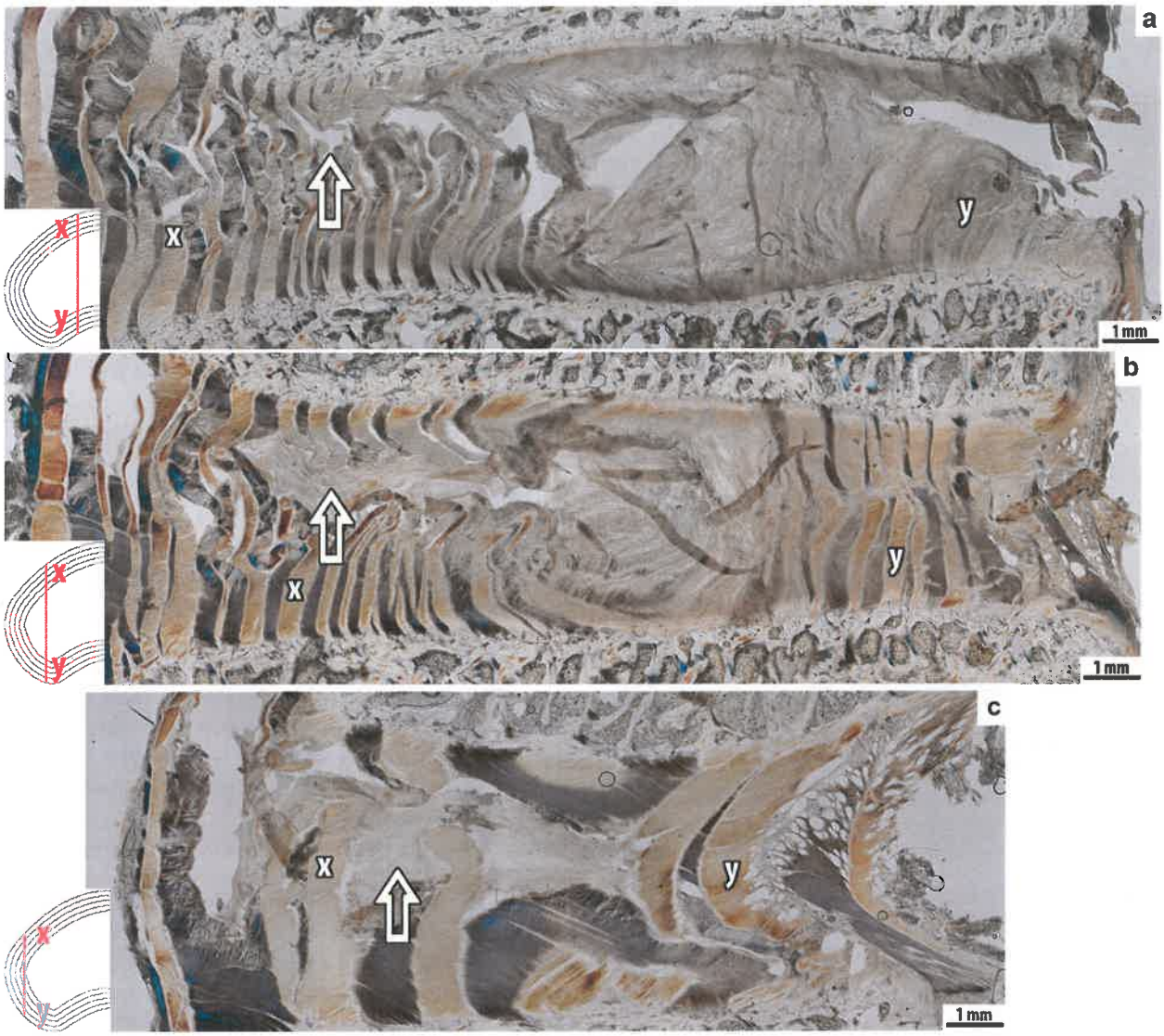

Fig. 6 A disc with mid-span annular direct tearing in both posterior and anterior regions. The direct tear can be seen anteriorly and anterolaterally (**a**, **b** *hollow arrows*) with extrusion of nuclear material evident anterolaterally (**b**), extending into the lateral annulus (**c**)

endplate tear shown in Fig. 7, there is no obvious mid-outer annular–endplate tear, which suggests that the initial failure was the direct mid-span tear. The endplate tearing probably relates to the substantial amount of nucleus extrusion, with the extruded material taking endplate material with it.

The low incidence of endplate tearing in the early stage samples (Table 1, samples 1–7) adds weight to the suggestion that endplate tearing is not part of the initiation of failure for high rate complex loading. The lower angle of flexion in the complex posture (7° instead of 10°) could be a factor, in combination with the more extreme shear created by this posture compromising other areas of the disc wall to such an extent that the endplate junction is no longer the weakest link. Note, nearly all of the endplate tearing was separation at the cement-line (as drawn in Fig. 2d, and shown in Fig. 7), i.e., without bone fragments attached. However, in two of the 11 discs with endplate tears (CL400 9 L56 and CL400 11 L34), a few slices did have bone attached in areas adjacent to a cement-line tear. We suspect that this bone damage could have occurred during processing of the thin section. But it does highlight the possibility of a rim lesion/bone fracture occurring under similar loading conditions if the bone is compromised or not as strong as a healthy young sheep.

Mechanically generated rim lesions, delaminations, and radiating tears have often been suggested as the first step in degeneration of the intervertebral joint complex [15–19].

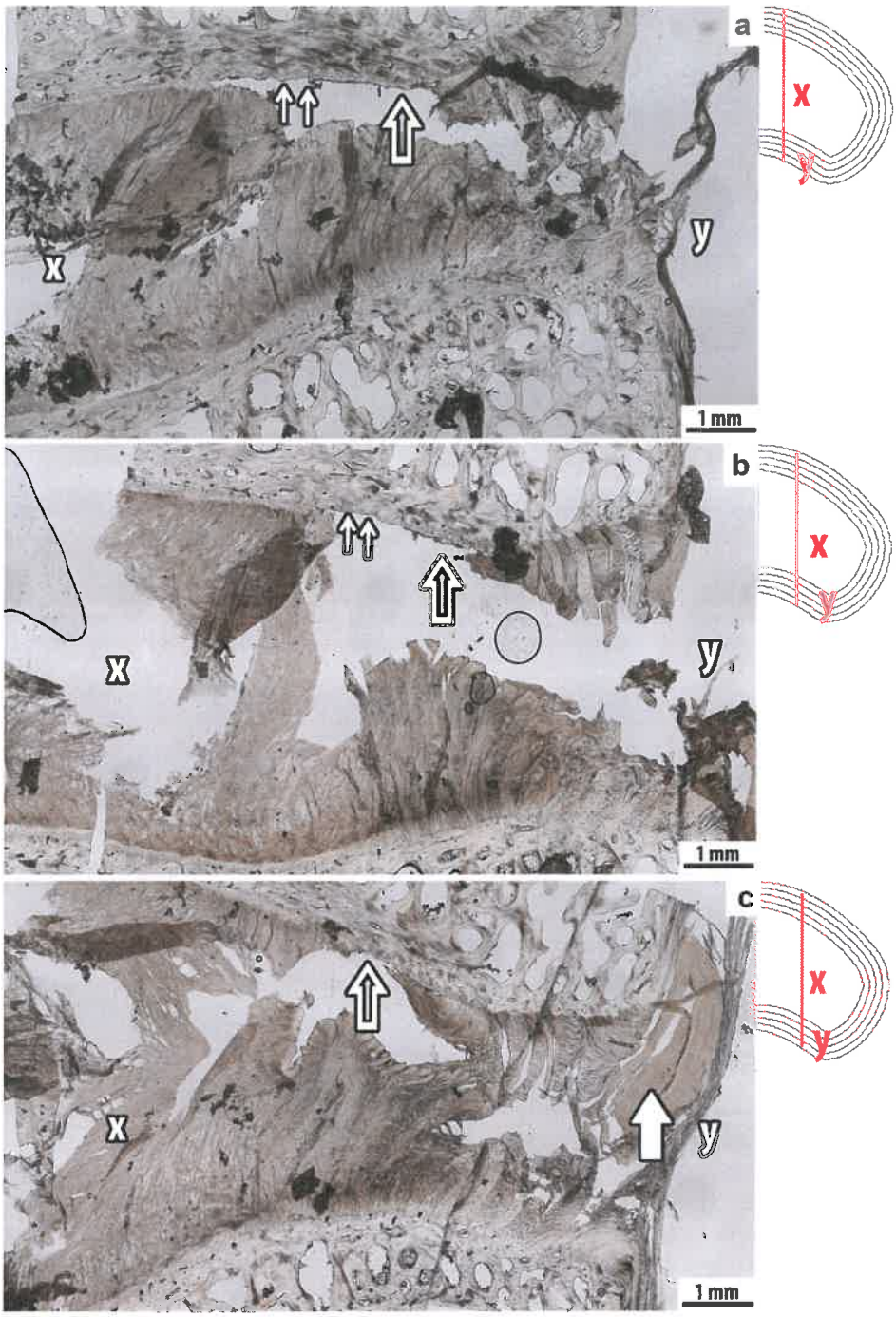

Fig. 7 A disc with disc–endplate tear in both the nucleus (*small arrows*) and annulus regions (*hollow arrow*) (**a**), connected to a mid-span annular direct tearing (**b**). The direct tear can also be seen posterolaterally (**c**), along with an isolated pocket of nuclear material contained within the posterior ligament (*solid arrow*)

Importantly, our present study has shown that with loading in a physiologic posture, it is possible to cause considerable mechanical derangement of this type. Previous studies have forewarned us of the disc being especially vulnerable to loading that is borne by one set of lamellae [20, 21].

Earlier studies adopting simple flexion have demonstrated non-significant trends of higher failure loads for more caudad discs (Part I and [3, 10]). In contrast, the difference is statistically significant between L12 and L56 for complex postures at both loading rates, suggesting the

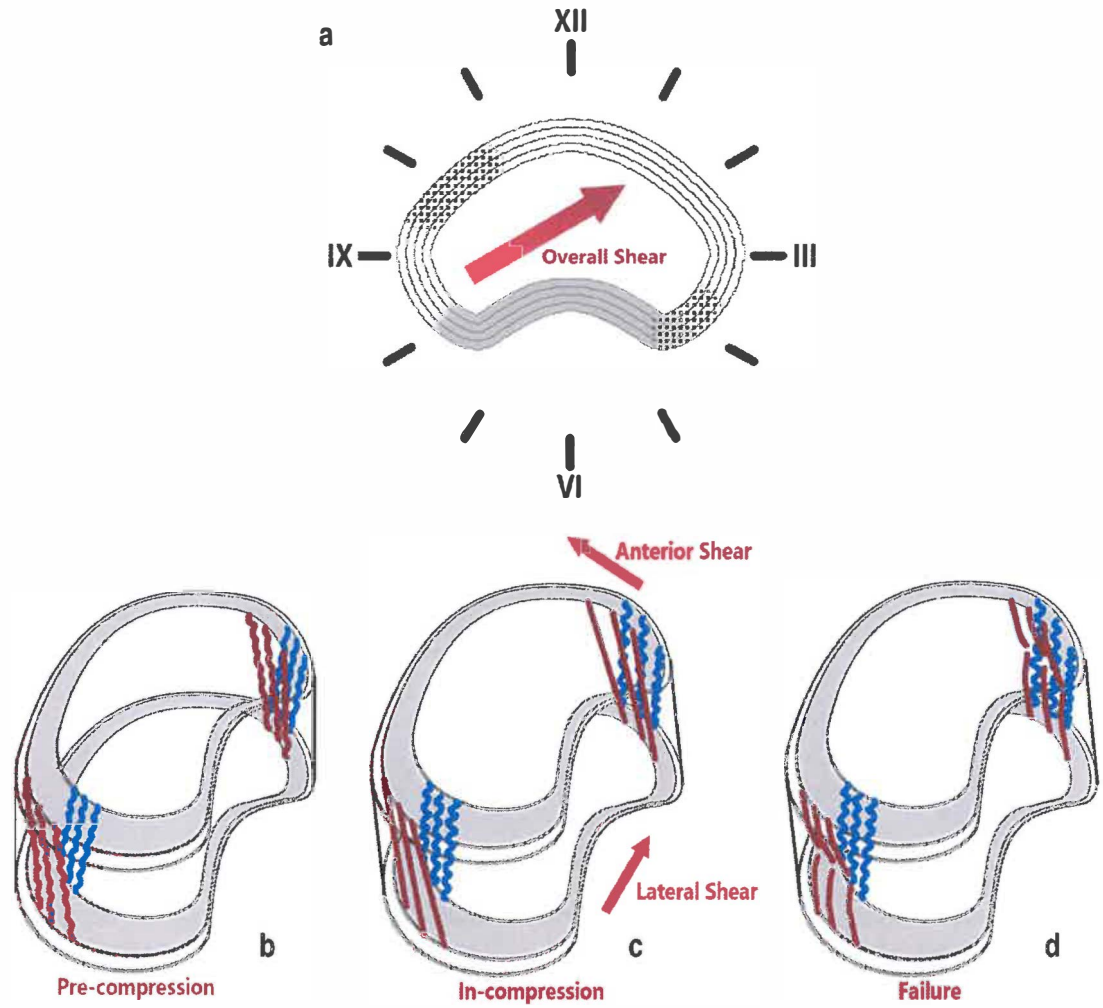

Fig. 8 **a** Regions of the disc indicated by a clock face; *shaded area* indicating the annulus region most affected by flexion, and the *dotted areas* showing the regions principally affected by shear. Two sets of counter-oblique fibres in a disc subjected to the complex posture are shown; relaxed (**b**), loaded (**c**) and failed (**d**). Note that the loading puts the fibres of one counter-oblique direction into tension, and possible failure

increased disc size is of more importance with the inclusion of shear.

In conclusion, multiple modes of damage are common when a segment is compressed in a complex posture, and its load bearing ability, already less than in a neutral or flexed posture, is further reduced with high rate loading. This study confirms the clinical observation that complex postures with loading render the disc more susceptible to failure [1, 22, 23], and that there is rationale for employing neutral postures along with engagement of core and trunk musculature in manual material handling activities.

Acknowledgements The authors gratefully acknowledge funding support from NuVasive and Medtronic (Australasia). We would also like to express our gratitude to Prof. Fengdong Zhao for supporting Zhi Shan's research visit to our laboratory.

Compliance with ethical standards

Conflict of interest The author(s) declare that they have no competing interests.

References

1. Marras WS, Lavender SA, Leurgans SE, Rajulu SL, Gary Allread W, Fathallah FA, Ferguson SA (1993) The role of dynamic three-dimensional trunk motion in occupationally-related low back disorders: the effects of workplace factors, trunk position, and trunk motion characteristics on risk of injury. Spine 18(5):617–628
2. Veres SP, Robertson PA, Broom ND (2010) ISSLS prize winner: how loading rate influences disc failure mechanics: a microstructural assessment of internal disruption. Spine 35(21):1897–1908. doi:10.1097/BRS.0b013e3181d9b69e

3. Wade KR, Robertson PA, Thambyah A, Broom ND (2015) 'Surprise' loading in flexion increases the risk of disc herniation due to annulus-endplate junction failure: a mechanical and microstructural investigation. Spine 40(12):891–901. doi:10.1097/BRS.0000000000000888
4. Dolan P, Adams MA (1993) The relationship between EMG activity and extensor moment generation in the erector spinae muscles during bending and lifting activities. J Biomech 26(4–5):513–522
5. Mannion AF, Adams MA, Dolan P (2000) Sudden and unexpected loading generates high forces on the lumbar spine. Spine 25(7):842–852
6. Oloyede A, Broom N (1993) Stress-sharing between the fluid and solid components of articular cartilage under varying rates of compression. Connect Tissue Res 30(2):127–141
7. Oloyede A, Flachsmann R, Broom ND (1992) The dramatic influence of loading velocity on the compressive response of articular cartilage. Connect Tissue Res 27(4):211–224
8. Race A, Broom ND, Robertson P (2000) Effect of loading rate and hydration on the mechanical properties of the disc. Spine 25(6):662–669
9. Wilke HJ, Kettler A, Claes LE (1997) Are sheep spines a valid biomechanical model for human spines? Spine 22(20):2365–2374
10. Wade KR, Robertson PA, Thambyah A, Broom ND (2014) How healthy discs herniate: a biomechanical and microstructural study investigating the combined effects of compression rate and flexion. Spine 39(13):1018–1028
11. Vernon-Roberts B, Moore RJ, Fraser RD (2007) The natural history of age-related disc degeneration: the pathology and sequelae of tears. Spine 32(25):2797–2804
12. van Heeswijk VM, Thambyah A, Robertson PA, Broom ND (2017) Posterolateral disc prolapse in flexion initiated by lateral inner annular failure: an investigation of the herniation pathway. Spine. doi:10.1097/BRS.0000000000002181
13. Aultman CD, Scannell J, McGill SM (2005) The direction of progressive herniation in porcine spine motion segments is influenced by the orientation of the bending axis. Clin Biomech 20(2):126–129
14. Berger-Roscher N, Casaroli G, Rasche V, Villa T, Galbusera F, Wilke HJ (2017) Influence of complex loading conditions on intervertebral disc failure. Spine 42(2):E78–E85. doi:10.1097/BRS.0000000000001699
15. Butler D, Trafimow JH, Andersson GBJ, McNeill TW, Huckman MS (1990) Discs degenerate before facets. Spine 15(2):111–113
16. Moore RJ, Crotti TN, Osti OL, Fraser RD, Vernon-Roberts B (1999) Osteoarthrosis of the facet joints resulting from anular rim lesions in sheep lumbar discs. Spine 24(6):519–525
17. Osti OL, Vernon-Roberts B, Fraser RD (1990) 1990 Volvo award in experimental studies: anulus tears and intervertebral disc degeneration: an experimental study using an animal model. Spine 15(8):762–767
18. Osti OL, Vernon-Roberts B, Moore R, Fraser RD (1992) Annular tears and disc degeneration in the lumbar spine: a post-mortem study of 135 discs. J Bone Joint Surg Ser B 74(5):678–682
19. Thompson RE, Pearcy MJ, Downing KJW, Manthey BA, Parkinson IH, Fazzalari NL (2000) Disc lesions and the mechanics of the intervertebral joint complex. Spine 25(23):3026–3035. doi:10.1097/00007632-200012010-00010
20. Farfan HF, Cossette JW, Robertson GH, Wells RV, Kraus H (1970) The effects of torsion on the lumbar intervertebral joints: the role of torsion in the production of disc degeneration. J Bone Joint Surg Am 52:468–497
21. Krismer M, Haid C, Rabl W (1996) The contribution of anulus fibers to torque resistance. Spine 21(22):2551–2557. doi:10.1097/00007632-199611150-00004
22. Fathallah FA, Marras WS, Parnianpour M (1998) The role of complex, simultaneous trunk motions in the risk of occupation-related low back disorders. Spine 23(9):1035–1042. doi:10.1097/00007632-199805010-00014
23. Kelsey JL, Githens PB, White AA (1984) An epidemiologic study of lifting and twisting on the job and risk for acute prolapsed lumbar intervertebral disc. J Orthop Res 2(1):61–66